Journal of Power Sources 269 (2014) 608–615

Contents lists available at ScienceDirect

Journal of Power Sources

journal homepage: www.elsevier.com/locate/jpowsour

Mixed organic compound-ionic liquid electrolytes for lithium battery electrolyte systems

M. Montanino [a, 1], M. Moreno [b], M. Carewska [b], G. Maresca [c], E. Simonetti [b], R. Lo Presti [b], F. Alessandrini [b], G.B. Appetecchi [b, *]

[a] ENEA, Agency for New Technologies, Energy and Sustainable Economic Development, UTTP-NANO, Piazza E. Fermi 1, Portici, Naples 80055, Italy
[b] ENEA, Agency for New Technologies, Energy and Sustainable Economic Development, UTRINN-IFC, via Anguillarese 301, Rome 00123, Italy
[c] Politecnico of Turin, Via Duca degli Abruzzi 24, Turin 10129, Italy

HIGHLIGHTS

- Electrolytes based on proper combination of ionic liquid with organic solvents.
- Enhanced safety in conjunction with fast ion transport properties.
- Conductivity approaching 10^{-3} S cm^{-1} at −20 °C.
- No flammability up to an organic compound mole fraction equal to 0.3.

ARTICLE INFO

Article history:
Received 19 March 2014
Received in revised form
16 June 2014
Accepted 3 July 2014
Available online 16 July 2014

Keywords:
Ionic liquids
Organic solvents
Mixed electrolytes
Lithium batteries

ABSTRACT

The thermal, transport, rheological and flammability properties of electrolyte mixtures, proposed for safer lithium-ion battery systems, were investigated as a function of the mole composition. The blends were composed of a lithium salt (LiTFSI), organic solvents (namely EC, DEC) and an ionic liquid (PYR_{13}TFSI). The main goal is to combine the fast ion transport properties of the organic compounds with the safe issues of the non-flammable and non-volatile ionic liquids. Preliminary tests in batteries have evidenced cycling performance approaching that observed in commercial organic electrolytes.

1. Introduction

The low safety is one of the main drawbacks of commercially available lithium-ion batteries because of the presence of flammable and volatile organic solvents in the electrolyte, e.g., namely ethylene carbonate (EC), dimethyl carbonate (DMC), diethyl carbonate (DEC), ethyl methyl carbonate (EMC) [1], resulting in possible fire and/or explosion of the electrochemical device. In addition, the safety issue dramatically decreases with increasing the battery size, this preventing commercialization for stationary (smart grid, renewable power source) and automotive (electric/hybrid vehicles) uses [2].

A promising approach for solving this problem is partial or total replacement of organic solvents (in the electrolytes) with a new class of fluid materials, acting as poorly flammable and/or flame retardant components, called ionic liquids (ILs). The latter are molten salts at room temperature or below, composed by organic cations combined with inorganic/organic anions [3,4]. The main advantages of ILs toward organic solvents are: low flammability, negligible vapor pressure, high chemical, electrochemical and thermal stability and, in some cases, hydrophobicity [3,4]. Despite these undoubtedly favorable characteristics, the ion conductivity of IL-based electrolytes is, however, still lower than that of organic solutions, with negative effect on the high rate performance of electrochemical devices. In this scenario, mixtures of ILs in combination with organic compounds have been proposed as electrolyte components for lithium batteries. Such an approach may represent a good compromise among fast ion transport properties (low viscosity) and improved safety (low flammability) of the resulting electrolyte [1,5–7]. Also, the incorporation of proper

* Corresponding author. Tel.: +39 06 3048 3924.
E-mail addresses: maria.montanino@enea.it (M. Montanino), gianni.appetecchi@enea.it, gianni.appetecchi@alice.it (G.B. Appetecchi).
[1] Tel.: +39 081 772 3320.

http://dx.doi.org/10.1016/j.jpowsour.2014.07.027
0378-7753/

organic compounds (such as vinyl carbonate), even in moderate amount (5–15 wt.%), into ionic liquid electrolytes was found to enhance the cycling battery performance [5–11].

In the last fifteen years, various ILs, in combination with organic solvents, have been proposed and tested as components for lithium battery electrolytes. Particularly, ionic liquids based on the bis(trifluoromethanesulfonyl)imide (TFSI) anion and the *N*-alkyl-*N*-methyl pyrrolidinium (PYR_{1A}) cation (the subscripts indicate the number of carbon atoms in the alkyl side chains) have been extensively studied because of their wide thermal and electrochemical stability and good ion conduction [12–14]. Furthermore, pyrrolidinium cations show some advantages if compared with the non-cyclic and unsaturated cyclic quaternary ammonium ones such as higher stability on reduction and better compatibility at the interface with electrodes because of the absence of acidic protons and double bonds [15,16].

This manuscript reports a physicochemical study on electrolyte mixtures composed by a lithium salt (LiTFSI), two of the most common organic solvents employed in lithium-ion battery systems (namely EC and DEC) and a pyrrolidinium TFSI ionic liquid (namely PYR_{13}TFSI). These quaternary mixed electrolytes were investigated in terms of thermal, transport, rheological and flammability properties by modulating the mole ratio of the different components. Also, the performance of the mixed electrolytes were tested in Li/$LiFePO_4$ and Li/$Li_4Ti_5O_{12}$ half-cells and compared with that of commercial organic solutions.

2. Experimental

2.1. Preparation of the electrolyte mixtures

The PYR_{13}TFSI ionic liquid was synthesized in our laboratory following a procedure route developed at ENEA and described in details elsewhere [17]. The lithium salt, LiTFSI (3 M, battery grade), was dried under high vacuum (>10^{-6} mbar) at 120 °C for 24 h. The organic solvents, EC and DEC (Merck, battery grade), were mixed in mole ratio equal to 1:1. Then, the EC/DEC blend was stirred with zeolites to reduce the initial water content (50 ppm) below 20 ppm and stored in presence of zeolites.

The electrolytic mixtures were prepared by mixing (in the proper mole fractions) LiTFSI, PYR_{13}TFSI and EC/DEC, which were successively stirred at 40–50 °C until to obtain homogeneous samples (e.g., full dissolution of LiTFSI in ionic liquid and organic solvents). Two different sample sets (Table 1) were prepared:

set A: binary mixtures (x)LiTFSI–$(1-x)PYR_{13}$TFSI where x and $(1-x)$ represent the mole fraction of the two components;
set B: quaternary mixtures (0.1)LiTFSI–$(0.9-x)PYR_{13}$TFSI–(x)EC/DEC where x is the overall mole fraction of EC/DEC (the EC:DEC mole ratio was fixed equal to 1:1).

The mixtures were prepared and characterized in a controlled environment dry room (humidity content below 10 ppm at 20 °C).

2.2. Water content

The water content was measured using the standard Karl Fisher method. The titrations were performed by an automatic Karl Fisher coulometer titrator (Mettler Toledo DL32) located inside the dry room. The Karl Fisher titrant was a one-component reagent (Hydranal 34836 Coulomat AG) provided from Aldrich.

2.3. Thermal analysis

The thermal measurements were performed using a TA Instruments (Model Q100) differential scanning calorimeter (DSC).

Table 1
Mole composition of the investigated electrolyte mixtures. The mole concentration values, with the respect to the Li^+, $(PYR_{13})^+$, $(TFSI)^-$ ion species, are reported.

	Mole fraction			Molarity/mole dm^{-3}		
	LiTFSI	PYR_{13}TFSI	EC/DEC	Li^+	$(PYR_{13})^+$	$(TFSI)^-$
Set A						
A1	0.1	0.9	–	0.37	3.32	3.69
A2	0.2	0.8	–	0.78	3.11	3.89
A3	0.3	0.7	–	1.23	2.88	3.11
Set B						
B1	0.1	0.8	0.1	0.40	3.17	3.57
B2	0.1	0.7	0.2	0.42	2.97	3.39
B3	0.1	0.6	0.3	0.46	2.78	3.24
B4	0.1	0.6	0.4	n.a.	n.a.	n.a.
B5	0.1	0.4	0.5	0.57	2.29	2.86
B6	0.1	0.3	0.6	n.a.	n.a.	n.a.
B7	0.1	0.2	0.7	0.73	1.46	2.19
B8	0.1	–	0.9	1.02	–	1.02

Hermetically sealed, aluminum pans were prepared in the dry room. In order to allow a complete crystallization [18], the materials were thermally annealed in the DSC instrument by repeatedly cycling and/or holding the samples at sub-ambient temperatures for varying time periods. Successively, the samples were cooled (10 °C min^{-1}) down to −140 °C and, then, heated (10 °C min^{-1}) up to 100 °C. The appearance of a cold recrystallization peak during the heating scan was taken as test of uncompleted crystallization of the sample.

2.4. Ionic conductivity

The ionic conductivity was determined by a conductivity meter AMEL 160 in the temperature range from −40 °C to 100 °C (60 °C for the set B samples) using a climatic test chamber (Binder GmbH MK53). The entire setup was controlled by a software developed at ENEA. The mixtures were housed (in the dry room) in sealed, glass conductivity cells (AMEL 192/K1) equipped with two porous platinum electrodes (cell constant equal to 1.0 ± 0.1 cm^{-1}). In order to fully crystallize the materials [18], the cells were immersed in liquid nitrogen for a few seconds and, then, transferred in the climatic chamber at −40 °C. After few minutes of storage at this temperature, the solid samples turned again liquid. This route was generally repeated until the samples remained solid at −40 °C. After a storage period at −40 °C for at least 18 h the conductivity of the materials was measured by running a heating scan at 1 °C h^{-1}.

2.5. Viscosity measurements

The viscosity measurements were carried out using a rheometer (HAAKE RheoStress 600) located in the dry room. The tests were performed from 20 °C to 80 °C (1 °C min^{-1} heating rate) in the 100 s^{-1} to 2000 s^{-1} rotation speed range. Measurements were taken after 10 °C steps.

2.6. Density measurements

The density measurements were performed from 90 °C to 20 °C at 10 °C step using a density meter (Mettler Toledo DE40) located in the dry room. The samples were previously degassed under vacuum at 50 °C overnight to avoid bubble formation during the cooling scan tests.

2.7. Flammability tests

The flammability tests were carried out on the electrolyte mixtures of set B (e.g., differing in the organic solvent content). The

samples, hold in a crucible exposed to air, were put in intimate contact with flames to evaluate their ignition ability.

2.8. Battery tests

The performance of the LiTFSI–PYR_{13}TFSI–EC/DEC mixed electrolytes were preliminarily tested in (cathode) Li/$LiFePO_4$ and (anode) Li/$Li_4Ti_5O_{12}$ half-cells. Composite electrodes were prepared by blending the active material ($LiFePO_4$ or $Li_4Ti_5O_{12}$), the electronic conductor (Super-P carbon) and the binder (PVdF) in cyclohexanone. The so-obtained slurry was cast onto aluminum ($LiFePO_4$) or copper ($Li_4Ti_5O_{12}$) foils, allowing the solvent removal at room temperature. Coin electrodes, having a 12 mm diameter and thickness ranging from 40 μm to 50 μm, were punched from the tapes. Finally, the electrodes were dried under vacuum at 110 °C overnight within the dry-room. The weight composition of electrodes resulted equal to 80:10:10 with an active material mass loading of 6.0 mg cm^{-2} and 7.0 mg cm^{-2} for cathodes and anodes, respectively. Taking into account for a reversible specific capacity of 170 mA h g^{-1} ($LiFePO_4$ and $Li_4Ti_5O_{12}$), this corresponds to capacity values of 1.0 mA h cm^{-2} ($LiFePO_4$) and 1.2 mA h cm^{-2} ($Li_4Ti_5O_{12}$), respectively.

The Li/$LiFePO_4$ and Li/$Li_4Ti_5O_{12}$ half-cells were fabricated within the dry room by housing in 2032 coin-type containers the sequence composed by a $LiFePO_4$ (or $Li_4Ti_5O_{12}$) electrode (12 mm diameter), a glass fiber separator (17 mm) loaded with electrolyte and a lithium disc anode (12 mm). The cycling performance was checked by a multichannel Maccor 4000 battery tester at 20 °C (within the dry room). The (galvanostatic) measurements were performed within the 2.0–4.0 V (cathode half-cells) and 1.0–2.5 V (anode half-cells) voltage range, respectively, at a current rate of 0.1 C (corresponding to 0.1 mA cm^{-2}).

3. Results and discussion

3.1. LiTFSI–PYR_{13}TFSI binary electrolyte mixtures

As a first sight, binary LiTFSI–PYR_{13}TFSI blend samples were investigated in terms of thermal and ion transport properties in order to evaluate the proper lithium salt concentration (indicated as mole fraction). Fig. 1 reports the DSC heating trace (panel A) and conductivity vs. temperature dependence (panel B) of the (x)LiTFSI–($1-x$)PYR_{13}TFSI mixtures. No exothermal feature due to cold crystallization is observed, indicating (as well as for the thermal traces of Fig. 2) the absence of supercooled and/or metastable phases within the mixtures. The neat ionic liquid exhibits an endothermic peak at 12 °C due to the melting of PYR_{13}TFSI [13,14,18]. The progressive addition of lithium salt moves the melting feature to lower temperatures due to the increase of disorder and the worst packing of ions because of the different steric hindrance of the $(PYR_{13})^+$ and Li^+ cations [18]. For instance, fusion temperature values close to −3 °C and below −5 °C are found for the A1 and A2 samples, respectively (Fig. 1A). On the other hand, a melting temperature increase up to 20 °C is seen at $x = 0.3$ (sample A3) as this LiTFSI mole fraction is closed to one of the eutectic mixture, e.g., (0.33)LiTFSI–(0.66)PYR_{13}TFSI, which, due to the very strong interactions among the Li^+ and $(TFSI)^-$ ions, is solid at ambient temperature [1,4,18]. In addition, the mixture A3 shows a further endothermic peak at about 0 °C, likely due to solid–solid phase transition.

The results depicted in panel B clearly show a decrease in conductivity (with the respect to the neat ionic liquid) with the progressive addition of lithium salt. This behavior is likely ascribable to increasing Li^+–$(TFSI)^-$ interactions, resulting in viscosity raise of the (x)LiTFSI–($1-x$)PYR_{13}TFSI mixtures [1,4,18]. However, the ionic conductivity is seen to exceed 10^{-3} S cm^{-1} already at room temperature for a LiTFSI mole fraction equal to 0.1 (sample B1), whereas a decay of about on order of magnitude is observed at $x = 0.3$ (B3). Therefore, accounting on the thermal and ion transport properties

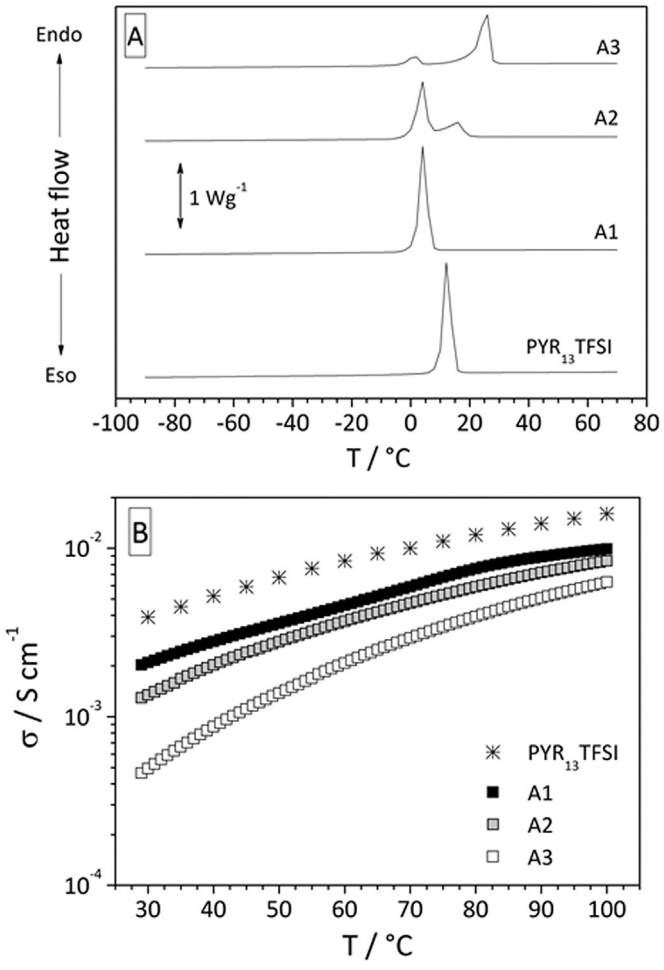

Fig. 1. DSC trace (panel A) and ionic conductivity vs. temperature dependence (panel B) of binary (x)LiTFSI–($1-x$)PYR_{13}TFSI electrolyte mixtures.

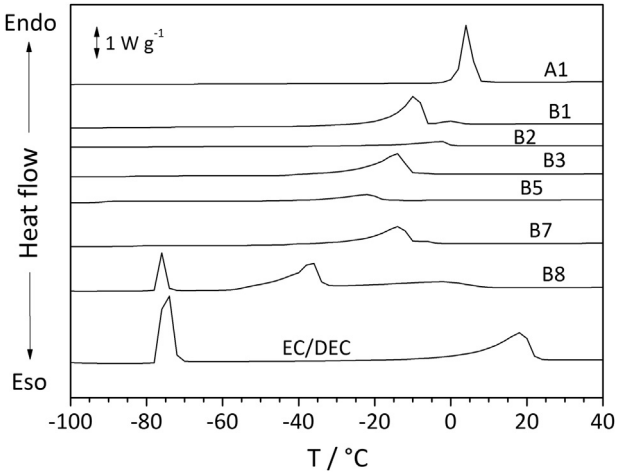

Fig. 2. DSC trace of quaternary (0.1)LiTFSI–(0.9 − x)PYR_{13}TFSI–(x)EC/DEC electrolyte mixtures. The EC:DEC mole ratio was kept equal to 1:1. Scan rate: 10 °C min^{-1}. The thermal trace of the EC/DEC blend is reported for comparison purpose.

of the LiTFSI-PYR_{13}TFSI mixtures, the LiTFSI mole fraction was fixed equal to 0.1.

3.2. *LiTFSI-PYR_{13}TFSI-EC/DEC quaternary electrolyte mixtures*

The (0.1)LiTFSI-(0.9-*x*)PYR_{13}TFSI-(*x*)EC/DEC quaternary electrolyte mixtures can be considered as derived from the (0.1)LiTFSI-(0.9)PYR_{13}TFSI binary samples by gradual replacement of the PYR_{13}TFSI ionic liquid with the analogous mole fraction of EC/DEC. Fig. 2 depicts the DSC heating trace of the (0.1)LiTFSI-(0.9-*x*)PYR_{13}TFSI-(*x*)EC/DEC mixtures. The thermal path of the (0.1)LiTFSI-(0.9)PYR_{13}TFSI (A1) and (0.1)LiTFSI-(0.9)EC/DEC (B8) samples and of the neat EC/DEC blend is reported for comparison purpose. A progressive shift of the endothermic feature, due to the melting of the samples, towards lower temperatures is observed with increasing the EC/DEC mole fraction (Table 2). This behavior may be addressed to loss in ionicity of the electrolytic mixture (i.e., EC and DEC are apolar compounds) as also evidenced by the Walden plot trend of Fig. 6. Furthermore, the presence of organic solvents interferes with the Li^+—$(TFSI)^-$ interactions, e.g., by solvating the high surface charge density lithium cations. The B8 mixture exhibits two endothermic features, located around −75 °C (e.g., displayed also in the DSC trace of the EC/DEC blend) and −37 °C (broader), addressed to the melting of DEC and EC, respectively [7]. Finally, a third, unexpected endothermic peak, even if weak and rather broad, is detected around −2 °C and is likely associated with the dissolution of the LiTFSI fraction which, upon melting of EC and DEC, remained undissolved (in EC/DEC) because of the limited solubility of the lithium salt in the organic solvents at low temperatures. Such a behavior, visually observed in solubility tests (results not shown) performed at different temperatures, is in good agreement with the conductivity results reported in Fig. 3. The glass transition temperature, as well as the melting point, is seen to decrease with the EC/DEC mole fraction (Table 2), resulting from a lower and lower ability of the electrolyte mixture to crystallize. Unexpectedly, the sample B7 does not seem to follow this trend, likely ascribable to rearrangement of the ion-molecule structural organization within the mixture. This issue agrees with the behavior exhibited from the viscosity and density values (Figs. 4 and 5) as a function of the organic solvent content (see later).

The ion transport properties of the (0.1)LiTFSI-(0.9-*x*)PYR_{13}TFSI-(*x*)EC/DEC quaternary mixtures are reported in Fig. 3 as conductivity vs. temperature dependence (panel A) and conductivity VTF plot (panel B). The A1 sample exhibits a steep conduction raise of about five orders of magnitude (e.g., from 10^{-8} S cm^{-1}, typical of solid IL electrolytes [13,14,18], to about 10^{-3} S cm^{-1}, comparable with liquid solution conductivity values) around 0 °C due to the fusion of the electrolytic sample [18], in good agreement with the DSC results reported in Fig. 1A. The progressive replacement of PYR_{13}TFSI with the corresponding moles of EC/DEC results in increasing conductivity (especially at low temperatures, i.e., below 0 °C) and in melting point decrease, this revealed by the conductivity plot knee shift (panel A) to lower temperature values. Such a behavior, in good agreement with the thermal measurement results (Fig. 2) and also evidenced from melting point comparison reported in Table 2, is once more ascribable to a decrease in ionicity and in entity of the Li^+—$(TFSI)^-$ interactions. At the same time, the increasing fraction of organic solvent progressively reduces the viscosity of the mixtures, as evidenced in Fig. 4, resulting in enhanced ion mobility and, therefore, faster transport properties. The gain in ion conduction is more evident at low temperatures because of the melting point decrease of the electrolytic mixtures

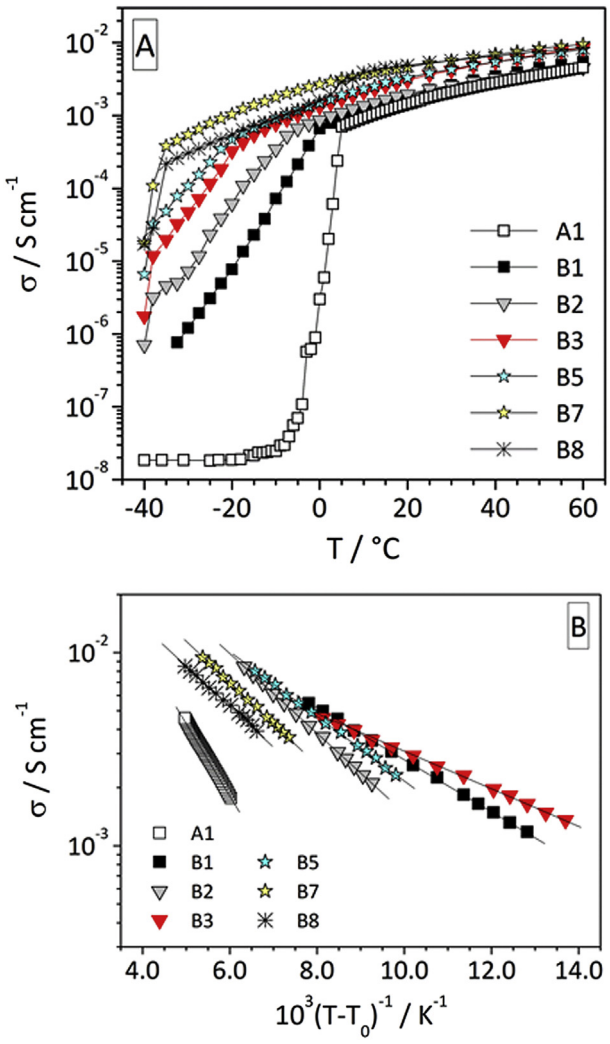

Fig. 3. Ionic conductivity vs. temperature dependence (panel A) and VFT conductivity plot (panel B) of quaternary (0.1)LiTFSI–(0.9 − *x*)PYR_{13}TFSI–(*x*)EC/DEC electrolyte mixtures. The EC:DEC mole ratio was kept equal to 1:1.

Table 2
Physicochemical properties, e.g., melting point (m.p.), ionic conductivity (σ), viscosity (η) and density (ρ), of the quaternary LiTFSI–PYR_{13}TFSI–EC/DEC electrolyte mixtures (set B) determined at 20 °C. The melting point values were obtained from the onset of the DSC traces whereas the ionic conductivity is also reported at −20 °C.

Sample	m.p./°C	T_g/°C	σ/S cm^{-1} (−20 °C)	σ/S cm^{-1} (20 °C)	η/mPa s (20 °C)	ρ/g cm^{-3} (20 °C)
A1	1.9 ± 0.5	–	$(1.9 \pm 0.1) \times 10^{-8}$	$(1.4 \pm 0.1) \times 10^{-3}$	127 ± 6	1.463 ± 0.001
B1	−15.7 ± 0.5	−75.9 ± 0.5	$(7.7 \pm 0.4) \times 10^{-6}$	$(1.8 \pm 0.1) \times 10^{-3}$	95 ± 5	1.451 ± 0.001
B2	−17.1 ± 0.5	−74.5 ± 0.5	$(6.1 \pm 0.3) \times 10^{-5}$	$(2.6 \pm 0.1) \times 10^{-3}$	61 ± 3	1.421 ± 0.001
B3	−24.7 ± 0.5	−82.7 ± 0.5	$(3.3 \pm 0.2) \times 10^{-4}$	$(3.0 \pm 0.2) \times 10^{-3}$	44 ± 2	1.410 ± 0.001
B4	−35.4 ± 0.5	−94.0 ± 0.5	$(5.7 \pm 0.3) \times 10^{-4}$	$(3.3 \pm 0.2) \times 10^{-3}$	35 ± 2	1.395 ± 0.001
B5	−24.1 ± 0.5	−81.4 ± 0.5	$(1.0 \pm 0.1) \times 10^{-3}$	$(4.6 \pm 0.2) \times 10^{-3}$	14.5 ± 0.7	1.341 ± 0.001
B6	−42.3 ± 0.5	–	$(5.5 \pm 0.3) \times 10^{-4}$	$(4.9 \pm 0.2) \times 10^{-3}$	5.2 ± 0.3	1.244 ± 0.001

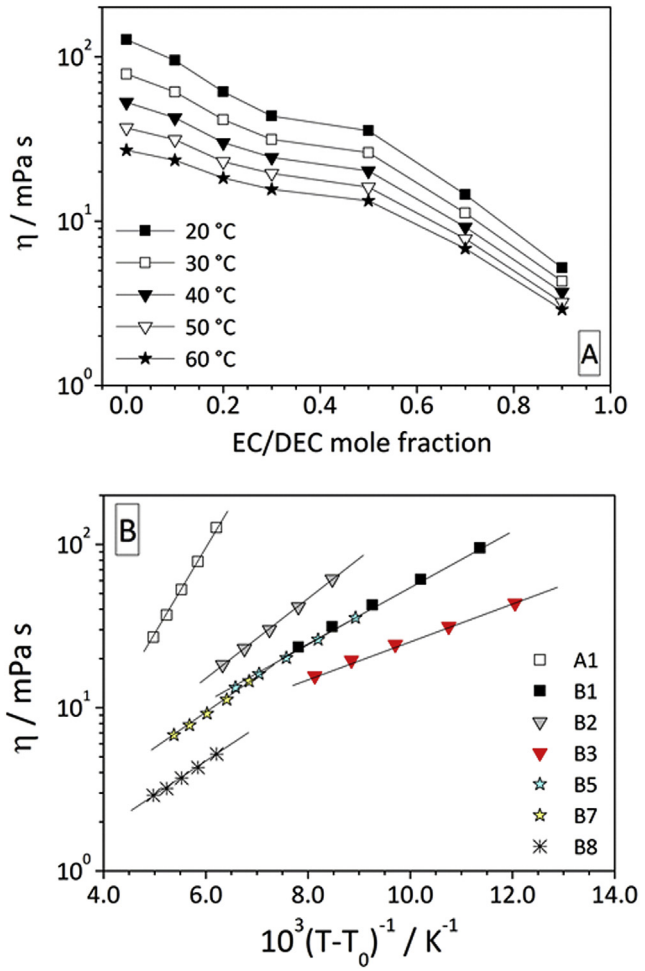

Fig. 4. Viscosity vs. EC/DEC mole fraction dependence (panel A) and VTF viscosity plot (panel B) of quaternary (0.1)LiTFSI–(0.9 – *x*)PYR_{13}TFSI–(*x*)EC/DEC electrolyte mixtures. The EC:DEC mole ratio was kept equal to 1:1.

with the EC/DEC content. For instance, a conductivity increase of more than two orders of magnitude, with respect to the organic-free mixture (open squares, A1), is observed at −20 °C even in presence of low EC/DEC mole fractions (solid squares, B1) whereas about four orders of magnitude are gained when the organic fraction achieves 0.3 (red triangles, B3). Conductivity values ($\geq 10^{-4}$ S cm^{-1}) of interest for practical applications are matched already at −20 °C and −30 °C for EC/DEC fractions equal to 0.3 and 0.5, respectively (Table 2). In the molten state, e.g., above 5 °C, the gain in conductivity due to organic solvent addition is more moderate, however, an increase of a factor 3 is detected at room temperature (Table 2). As it clearly results from panel A of Fig. 3, no improvement in ion conduction is observed for EC/DEC mole fractions larger than 0.7 (B7), this suggesting that, at high organic solvent contents, the presence of the ionic liquid does not affect the transport properties because the lithium salt is completely coordinated by the EC and DEC molecules. Finally, an unexpected behavior is exhibited by the organic (0.1)LiTFSI–(0.9)EC/DEC mixture (black stars, B8), which shows lower conductivity values (Table 2) with respect to the sample B7 (yellow stars) at low temperatures (e.g., up to 0 °C). This is due to partial precipitation of the lithium salt (upon melting of the sample B8) due to the limited solubility of LiTFSI in EC/DEC below room temperature, with consequent decrease of the charge carrier number (e.g., focusing that the measurements were carried out through a heating scan from −40 °C). No appreciable precipitation of lithium salt was observed in the other electrolytic mixtures. Above 2 °C the conductivity plot of the sample B8 displays a modest, but step, increase as a consequence of full dissolution of the lithium salt (which results more soluble in EC/DEC) and, above 5 °C, matches the conduction values of the mixture B7. This issue, visually observed in various solubility tests run as a function of the temperature, is in agreement with the DSC results of Fig. 2.

The ion conduction vs. temperature dependence of the (0.1) LiTFSI–(0.9 – *x*)PYR_{13}TFSI–(*x*)EC/DEC mixtures as reported in Fig. 3A follows, in the molten state, a VTF behavior [19–21], typical of amorphous ionically-conducting materials and generally observed in ionic liquid electrolytes [14,22,23]. This is confirmed by the straight-line trend exhibited from the conductivity diagrams reported in panel B of Fig. 3 as a function of 10^3 $(T - T_0)^{-1}$ accordingly to the equation:

$$\sigma = AT^{-1/2} \exp\left(-\frac{B}{T - T_0}\right) \quad (1)$$

where *A* and *B* are parameters correlated to the charge carrier number and the activation energy, respectively, whereas T_0 represents the ideal glass transition temperature. Only the data obtained at temperature ≥10 °C, i.e., where the mixture samples are in the molten state, are reported. The incorporation of EC/DEC results in slope decrease of the VTF diagrams with respect to the sample A1,

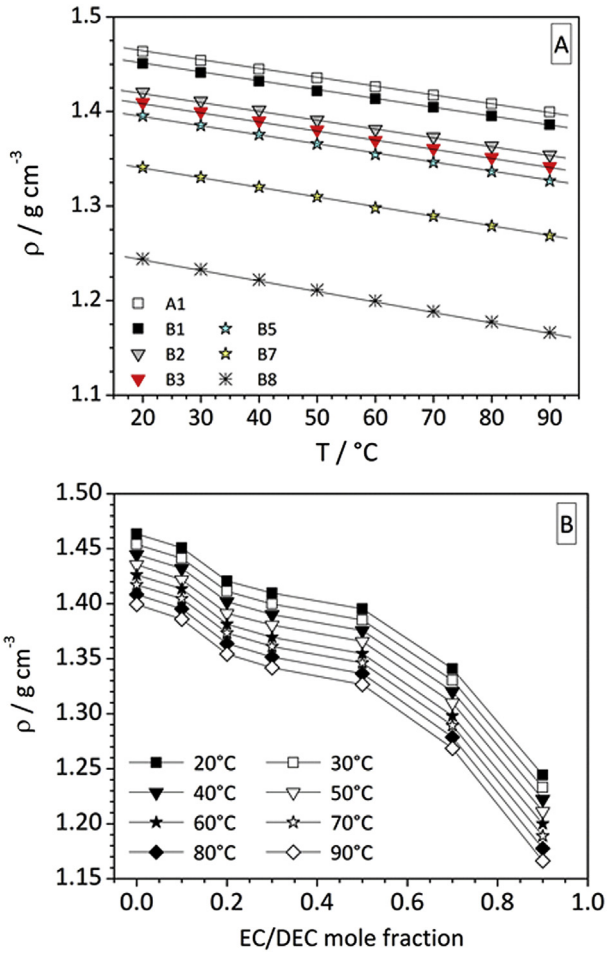

Fig. 5. Density vs. temperature (panel A) and mole fraction (panel B) dependence of quaternary (0.1)LiTFSI–(0.9 – *x*)PYR_{13}TFSI–(*x*)EC/DEC electrolyte mixtures. The EC:DEC mole ratio was kept equal to 1:1.

suggesting lower activation energy for the ion transport through the quaternary mixtures. At high EC/DEC contents ($x \geq 0.5$, sample B5), the mixtures show a higher slope, even if lower than the organic-free B1 sample ($x = 0$). This unexpected behavior is likely ascribable to the "*free volume*" (V_v), e.g., representing the available void space for the ion transferring through the mixed mixtures [24], which may play a major role on ion transport properties. The ion movement occurs if the *free volume* medium value, V_c^m, exceeds a critical volume, V_c, accordingly to the following equation:

$$V_c^m = V_0\alpha(T - T_0) \quad (2)$$

where α and V_0 represent the free volume extension coefficient and the free volume at temperature $= T_0$, respectively. Equation (2) shows a linear dependence of V_c^m on $(T - T_0)$, as well as evidenced for the ion conduction, suggesting how the ion transport through the quaternary mixtures is correlated to the formation of vacancies, e.g., able to allow the ion transferring, due to the statistical distribution of void volumes. This issue is seen to change with the EC/DEC mole fraction within the electrolyte blends.

The results obtained from the rheological measurements are illustrated in Fig. 4 as viscosity vs. EC/DEC mole fraction dependence (panel A) and viscosity VTF plot (panel B). Only the data obtained at temperature ≥20 °C, i.e., where the IL mixtures showed Newtonian behavior, are reported. In agreement with the transport properties, the viscosity values are seen to decrease with the increase in temperature and in organic compound content (panel A), resulting in enhanced ion mobility. A more pronounced viscosity decay with the EC/DEC mole fraction is observed above $x = 0.5$ (B5). At $x < 0.5$ the organic compound molecules are mainly busy in the ion coordination (particularly of the Li^+ cations), resulting in lower reduction of the "*viscous drag*" within the electrolyte. Conversely, for $x > 0.5$ the increase of the EC/DEC content leads to increasing fraction of *free* solvent, e.g., not involved in the ion solvation, this resulting in more remarkable decay of the viscous friction among ions and organic molecules. The VTF diagrams, reported in panel B of Fig. 4, exhibit a linear behavior with analogous slope trend with respect to the one observed for the VTF conductivity plots (panel B of Fig. 3). Once more, this indicates that the ion transport properties of the (0.1)LiTFSI–(0.9 − x)PYR_{13}TFSI–(x)EC/DEC electrolytes are mainly governed by the available *free volume* and the *viscous drag* within the mixtures.

Fig. 5 reports the results obtained from the density measurements performed on the (0.1)LiTFSI–(0.9 − x)PYR_{13}TFSI–(x)EC/DEC quaternary mixtures. A linear decrease with the temperature, independently on the EC/DEC mole fraction, is observed (panel A). This behavior, commonly encountered in other ionic liquid electrolytes [1,14,17,22,23], is ascribable to worse ion-molecule packing, e.g., not depending on the organic solvent content, due the increasing thermal motions. A reduction in density, independently on the temperature, is also recorded with the increase of the EC/DEC content (panel B), suggesting that ion coordination by organic solvent molecules depletes the packing within the electrolyte mixtures. However, three different behavior regions can be distinguished. At low ($0 \leq x < 0.2$) EC/DEC mole fractions the Li^+ cations are mainly coordinated by the $(TFSI)^-$ anions and even moderate additions of organic compounds, e.g., competitors in the coordination of the lithium ions, result in remarkable ion-molecule structural organization changes within the electrolyte mixture, resulting in pronounced density decrease. At intermediate ($0.2 < x < 0.5$) mole fractions the Li^+ cations are coordinated both

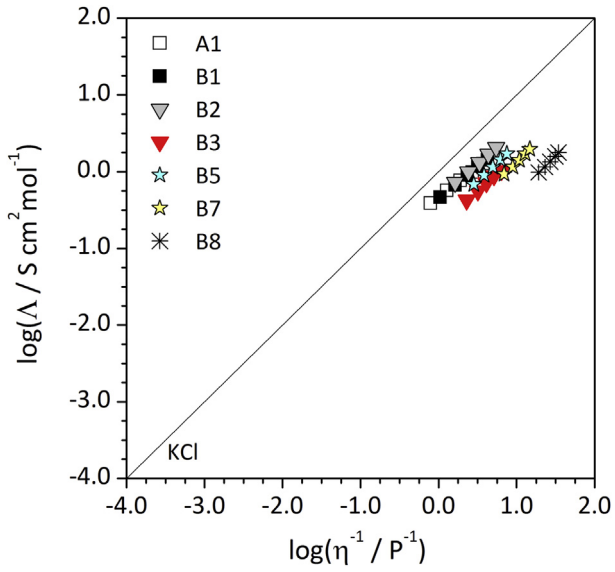

Fig. 6. Walden plot of quaternary (0.1)LiTFSI–(0.9 − x)PYR_{13}TFSI–(x)EC/DEC electrolyte mixtures. The EC:DEC mole ratio was kept equal to 1:1. The solid straight line, referred to a 0.01 N KCl solution, fixes the position of the ideal Walden line.

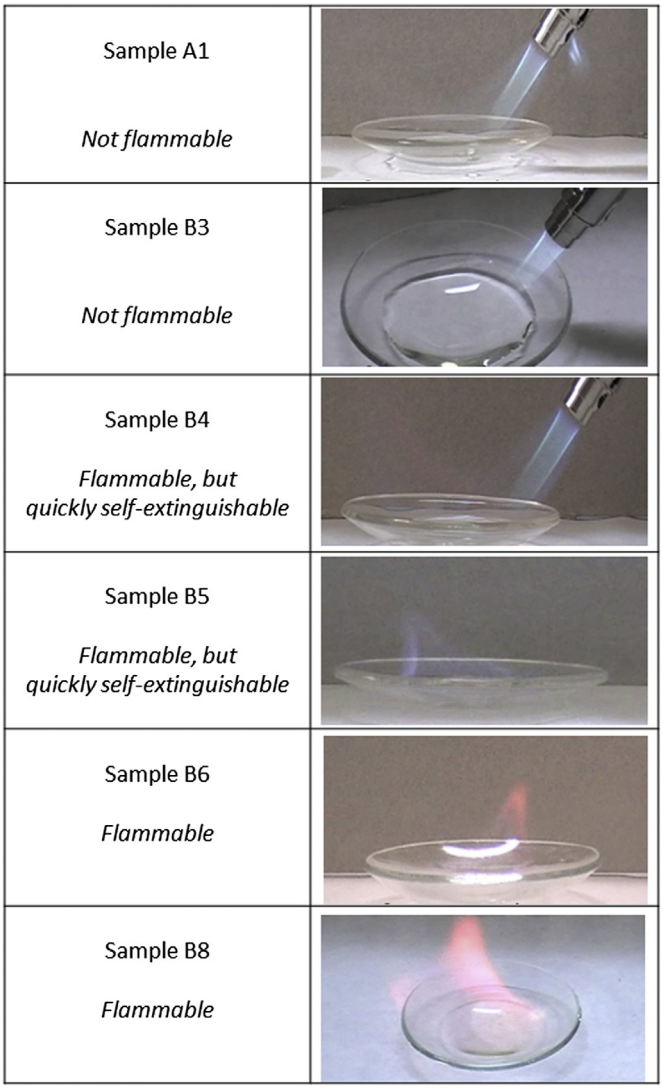

Fig. 7. Flammability test carried out on quaternary (0.1)LiTFSI–(0.9 − x)PYR_{13}TFSI–(x) EC/DEC electrolyte mixtures. The EC:DEC mole ratio was kept equal to 1:1.

by the organic molecules and the $(TFSI)^-$ anions and, consequently, further incorporation of EC/DEC does not produce relevant structural changes, leading to moderate density reduction. Finally, at high ($0.5 < x \leq 1$) EC/DEC mole fractions the Li^+ cations are mainly solvated by the organic molecules and, therefore, the density of the quaternary mixture results (again) remarkably affected by further addition of the less dense EC/DEC (now *free* solvents) blend (1.15 g cm^{-3} at 25 °C) with respect to the $PYR_{13}TFSI$ ionic liquid (1.43 g cm^{-3} at 25 °C [13]).

The *ionicity* of the (0.1)LiTFSI–(0.9 – *x*)$PYR_{13}TFSI$–(*x*)EC/DEC quaternary electrolyte mixtures was qualitatively investigated through the Walden rule [25,26]:

$$\Lambda = \frac{k}{\eta} \tag{3}$$

where Λ is the molar conductivity (calculated taking into account the molar concentration of the LiTFSI lithium salt and the $PYR_{13}TFSI$ ionic liquid), η is the viscosity and k is a temperature dependent constant. The log Λ vs. $\log\eta^{-1}$ dependence of the investigated samples is plotted in Fig. 6. The solid straight line (through the origin) is referred to a 0.01 N KCl aqueous solution; this system, known to be fully dissociated and to have ions of equal mobility [25], was used as the calibration point (e.g., ideal Walden line). From Table 1 it is seen how the quaternary LiTFSI–$PYR_{13}TFSI$–EC/DEC mixtures show a progressive increase in lithium salt mole concentration even if the LiTFSI mole fraction is kept fixed equal to 0.1. This behavior is ascribable to progressive replacement of the heavier $PYR_{13}TFSI$ ionic liquid with lighter EC and DEC organic molecules. The (0.1)LiTFSI–(0.9 – *x*)$PYR_{13}TFSI$–(*x*)EC/DEC mixtures are seen to lie below the ideal line, behaving as "good ionic liquid electrolytes" [25–27], e.g., mostly consisting of independently mobile ions, up to an EC/DEC mole fraction equal to 0.2 (sample B2). As expected, the increase of the organic solvent content results in progressive lowering of the Walden plot below the ideal line, suggesting progressive lack in ionicity due to raising amounts of apolar compounds.

Ignition tests (Fig. 7) have shown no flammability for the (0.1) LiTFSI–(0.9 – *x*)$PYR_{13}TFSI$–(*x*)EC/DEC electrolytic mixtures up to EC/DEC mole fraction equal to 0.3 (sample B3). An organic fraction increase up to 0.5 (B5) makes the mixtures slightly flammable, but the flame suddenly disappears when the source of ignition is removed, indicating that the ionic liquid is able to protect EC and DEC from combustion. A further raise in organic compound content makes flammable the electrolytic mixture.

Finally, the performance of the electrolyte mixtures was investigated in Li/$LiFePO_4$ and Li/$Li_4Ti_5O_{12}$ half-cells and compared with that of $LiPF_6$(1 M)–EC/DEC (1:1 in weight) commercial (Merck, LP40, battery grade) solutions. The sample B3 was selected as the mixed ionic liquid-organic solvent electrolyte. The results are reported as voltage vs. capacity profiles in Fig. 8 (Li/$LiFePO_4$) and 9 (Li/$Li_4Ti_5O_{12}$). The voltage profile feature reflects the reversible charge (lithium removal)-discharge (lithium uptake) cycling behavior of the $LiFePO_4$ [28] and $Li_4Ti_5O_{12}$ [29] materials, characterized by a well-defined flat plateau evolving at around 3.5 V ($LiFePO_4$) and 1.5 V ($Li_4Ti_5O_{12}$) vs. Li/Li^+, respectively, both in commercial (panel A of Figs. 8 and 9) and B3 (panel B) electrolyte. The reversible capacity is seen to achieve 90% of the theoretical value, both in Li/$LiFePO_4$ and Li/$Li_4Ti_5O_{12}$ half-cells containing the mixed electrolyte B3, corresponding to 153 mA h g^{-1}. The Li/$LiFePO_4$ cells display a charge/discharge efficiency leveling at 100% starting from the 1st

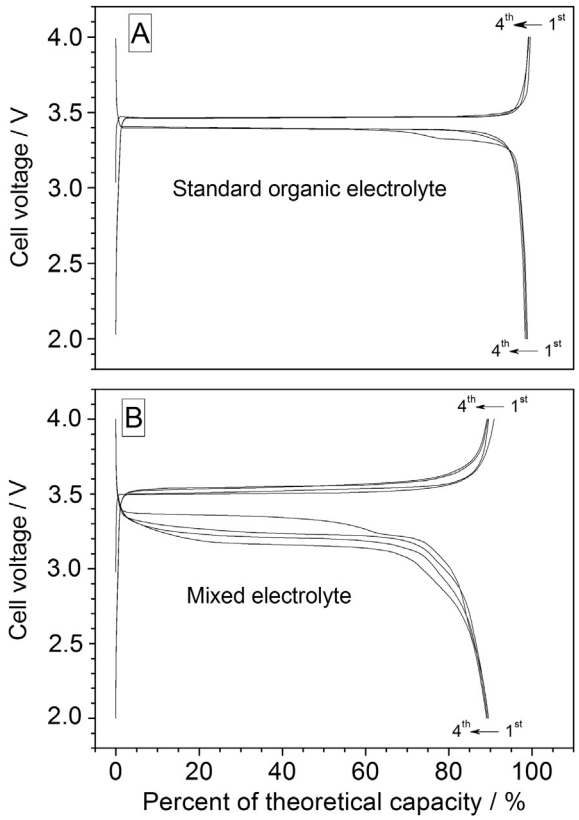

Fig. 8. Voltage vs. charge/discharge capacity profiles of Li/$LiFePO_4$ half-cells in commercial $LiPF_6$–EC/DEC (panel A) and mixed B3 (panel B) electrolyte. Current rate: 0.1 C (0.1 mA cm^{-2}). Temperature: 20 °C.

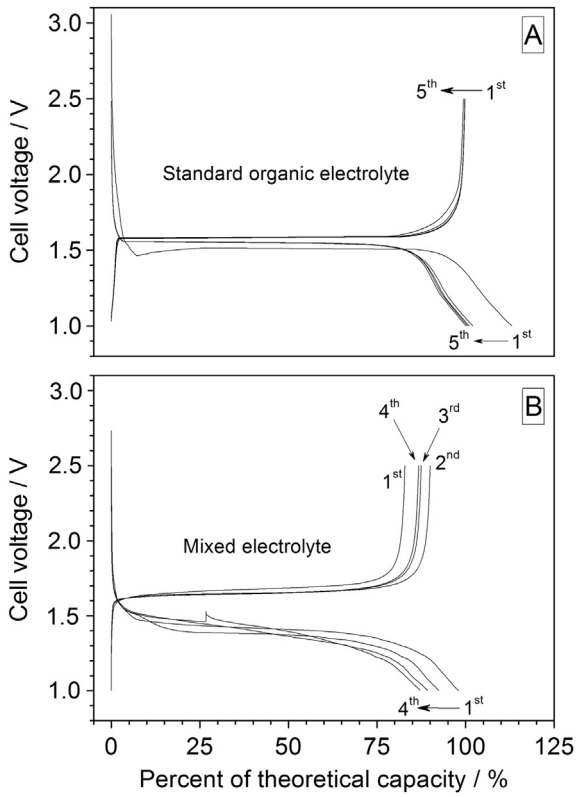

Fig. 9. Voltage vs. charge/discharge capacity profiles of Li/$Li_4Ti_5O_{12}$ half-cells in commercial $LiPF_6$–EC/DEC (panel A) and mixed B3 (panel B) electrolyte. Current rate: 0.1 C (0.1 mA cm^{-2}). Temperature: 20 °C.

cycle. Conversely, the Li/$Li_4Ti_5O_{12}$ half-cells (Fig. 9) show a first cycle irreversible capacity close to 11% and 15% in standard electrolyte (panel A) and in the mixture B3 (panel B), respectively. However, the coulombic efficiency is found to leveling 100% after a few cycles. It is to note, for the cells containing the mixture B3, a reversible capacity increase from 83% to 90% in the 2nd cycle, likely ascribable to progressive improvement in wettability and/or (more viscous) electrolyte loading of the $Li_4Ti_5O_{12}$ electrode.

4. Conclusions

This paper deals on physicochemical investigation of mixed electrolytes, based on the PYR_{13}TFSI ionic liquid and the EC and DEC solvents, proposed for safer lithium-ion battery systems. The purpose is combining negligible volatility and no flammability of ionic liquid materials with fast transport properties typical of small steric hindrance organic compounds.

The results have shown that the (0.1)LiTFSI–(0.6)PYR_{13}TFSI–(0.3)EC/DEC mixture may represent a proper compromise among good ionic conductivity, low melting temperature and safety. The selected electrolyte exhibits ion conduction above 10^{-4} S cm^{-1} and 10^{-3} S cm^{-1} at −20 °C and 0 °C, respectively, in conjunction with no flammability even in intimate contact with ignition sources. The transport properties appear well correlated with the rheological behavior. The variation of the ionic liquid/organic compound mole ratio leads to changes in ion-molecule structural organization and ionicity of the mixed electrolytes. Preliminary battery tests run in Li/$LiFePO_4$ and Li/$Li_4Ti_5O_{12}$ half-cells have evidenced cycling performance approaching that observed in commercial organic electrolytes.

Acknowledgments

The financial support of the Italian Ministry of Economic Development (MSE), within the Program Agreement ENEA-MSE on Electric System Research, is kindly acknowledged.

References

[1] G.B. Appetecchi, M. Montanino, S. Passerini, in: A.E. Vissser, N.J. Bridges, R.D. Rogers (Eds.), Ionic Liquids: Science and Applications, ACS Symposium Series, vol. 1117, Oxford University Press, Inc., American Chemical Society, Washington, DC, USA, 2013.
[2] T.M. Bandhauer, S. Garimella, T.F. Fuller, J. Electrochem. Soc. 158 (2011) R1.
[3] J.R.D. Rogers, K.R. Seddon, Ionic Liquids: Industrial Application to Green Chemistry, in: ACS Symposium Series, vol. 818, American Chemical Society, Washington, 2002.
[4] H. Ohno (Ed.), Electrochemical Aspects of Ionic Liquids, John Wiley & Sons Inc., Hoboken, New Jersey, 2005.
[5] A. Guerfi, M. Dontigny, P. Charest, M. Petitclerc, M. Lagacé, A. Vijh, K. Zaghib, J. Power Sources 195 (2010) 845.
[6] R.-S. Kuhnel, N. Böckenfeld, S. Passerini, M. Winter, A. Balducci, Electrochim. Acta 56 (2011) 4092.
[7] A. Lex-Balducci, W.A. Henderson, S. Passerini, Chapter 4, in: J. Yuan, X. Liu, H. Zhang (Eds.), Lithium-ion Batteries: Advanced Materials and Technologies, Electrolytes for Lithium Batteries, CRC Press, 2011, print, ISBN 978-1-4398-4128-0. eBook ISBN 978-1-4398-4129-7.
[8] Z. Zhang, H. Zhou, L. Yang, K. Tachibana, K. Kamijima, J. Xu, Electrochim. Acta 53 (2008) 4833.
[9] J. Jin, H.H. Li, J.P. Wei, Z. Zhou, J. Yan, Electrochem. Commun. 11 (2009) 1500.
[10] A. Lewandowski, A. Świderska-Mocek, I. Acznik, Electrochim. Acta 55 (2010) 1990.
[11] J.-A. Choi, E.-G.- Shim, B. Scrosati, D. Won Kim, Bull. Korean Chem. Soc. 31 (11) (2010) 3190.
[12] D.R. McFarlane, J. Sun, J. Golding, P. Meakin, M. Forsyth, Electrochim. Acta 45 (2000) 1271.
[13] G.B. Appetecchi, M. Montanino, D. Zane, M. Carewska, F. Alessandrini, S. Passerini, Electrochim. Acta 54 (2009) 1325.
[14] G.B. Appetecchi, M. Montanino, M. Carewska, M. Moreno, F. Alessandrini, S. Passerini, Electrochim. Acta 56 (2011) 1300.
[15] Z.B. Zhou, H. Matsumoto, K. Tatsumi, Chem. Eur. J. 12 (2006) 2196.
[16] V.R. Koch, C. Nanjundiah, G.B. Appetecchi, B. Scrosati, J. Electrochem. Soc. 142 (1995) L116.
[17] M. Montanino, F. Alessandrini, S. Passerini, G.B. Appetecchi, Electrochim. Acta 96 (2013) 124.
[18] W.A. Henderson, S. Passerini, Chem. Mater. 16 (2004) 2881.
[19] H. Vogel, Phys. Z 22 (1921) 645.
[20] G.S. Fulcher, J. Am. Chem. Soc. 8 (1925) 339.
[21] G. Tamman, W. Hesse, Z. Anorg. Allg. Chem. 156 (1926) 245.
[22] M. Montanino, M. Moreno, F. Alessandrini, G.B. Appetecchi, S. Passerini, Q. Zhou, W.A. Henderson, Electrochim. Acta 60 (2012) 163.
[23] M. Moreno, M. Montanino, M. Carewska, G.B. Appetecchi, S. Jeremias, S. Passerini, Electrochim. Acta 99 (2013) 108.
[24] W. Beichel, Y. Yu, G. Dlubek, R. Krause-Rehberg, J. Pionteck, D. Pfefferkorn, S. Bulut, D. Bejan, C. Friedrich, I. Krossing, Phys. Chem. Chem. Phys. 15 (2013) 8821.
[25] Z.-B. Zhou, H. Matsumoto, K. Tatsumi, Chem. Eur. J. 11 (2005) 752.
[26] C.A. Angell, W. Xu, M. Yoshizawa, A. Hayashi, J.-P. Belieres, in: H. Ohno (Ed.), Ionic Liquids: the Front and Future of Materials Development (in Jpn), CMC, Tokyo, 2003, p. 43.
[27] D.R. MacFarlane, M. Forsyth, E.I. Izgorodina, A.P. Abbott, G. Annat, K. Fraser, Phys. Chem. Chem. Phys. 11 (25) (2009) 4962.
[28] N. Ravel, J.B. Goodenough, S. Besner, M. Gauthier, M. Armand, in: Abstracts of the Electrochemical Society and the Electrochemical Society of Japan Meeting (Abstract 127), Honolulu, vol. 99, 1997, 2.
[29] J. Mun, Y.S. Jung, T. Yim, H.Y. Lee, H.-J. Kim, Y.G. Kim, S.M. Oh, J. Power Sources 194 (2009) 1068.